

CONF-770706--26

TITLE: OIL SHALES UNDER DYNAMIC STRESS

AUTHOR(S): B. W. Olinger

SUBMITTED TO: 6th AIRAPT International High Pressure Conference,
University of Colorado, Boulder, Colorado,
July 25-29, 1977

By acceptance of this article for publication, the publisher recognizes the Government's (license) rights in any copyright and the Government and its authorized representatives have unrestricted right to reproduce in whole or in part said article under any copyright secured by the publisher.

The Los Alamos Scientific Laboratory requests that the publisher identify this article as work performed under the auspices of the USERDA.


los alamos
scientific laboratory
of the University of California
LOS ALAMOS, NEW MEXICO 87545

An Affirmative Action/Equal Opportunity Employer

NOTICE
This report was prepared as an account of work sponsored by the United States Government. Neither the United States nor the United States Energy Research and Development Administration, nor any of their employees, nor any of their contractors, subcontractors, or their employees, make any warranty, express or implied, or assume any legal liability or responsibility for the accuracy, completeness or usefulness of any information, apparatus, product or process disclosed, or represents that its use would not infringe privately owned rights.

DISTRIBUTION OF THIS DOCUMENT IS UNLIMITED

pen

OIL SHALES UNDER DYNAMIC STRESS

Dart Olinger

Los Alamos Scientific Laboratory
Los Alamos, NM 87545

INTRODUCTION

The Los Alamos Scientific Laboratory has recently begun development of techniques to fracture oil shale beds hundreds of meters beneath the earth's surface. The resulting shale fragment sizes must permit efficient in-place retorting of organic material from the shale. The initial phase of the program requires the determination of the properties of the shales under dynamic compression. These properties and those of the proposed explosives form the base for computer modeling of field events. Here, the dynamic properties of oil shales and the experimental techniques used to determine them are discussed.

ELASTIC PROPERTIES

The determination of the elastic constants of oil shales is the first step towards understanding the shale's response to both static and dynamic stresses. Previous investigators have treated the shale as a transverse isotropic solid (1); (2), (3) since it consists of fine bedding planes each of which is nearly homogenous and has properties that are repetitive in the direction perpendicular to the beds.

The shales studied have come from the Anvil Points Mine, near Rifle, Colorado. Thirteen shale samples spanning the density range from 1.5 to 2.5 Mg/m³ were ground and x-ray patterns were taken of each. Table 1 lists the minerals found in the samples. The assemblages were restricted to only five minerals--dolomite, quartz, analcime, calcite and albite. Compared to reports of minerals from other oil shales, these shales were

unique in the large percentage of analcime (analcite) present, the sparsity of calcite and the absence of diffraction patterns from others such as pyrite, illite, and microcline. Thin sections clearly show the presence of pyrite, though only in small amounts concentrated within certain layers. Once the minerals were identified and their volume percentages estimated by making comparisons with control mixes of pure minerals, it was found that the kerogen volume content could be readily estimated from the total density of the shale samples and the calculated density of the mineral assemblages, which was restricted to a narrow range of from 2.6 to 2.7 Mg/m³ (Table I). The analcime content lowered the density of the shales slightly making the oil yield for a given density lower than what is normal for Green River oil shales (4).

The shales were prepared for sound speed measurements by cutting them into plates 30 to 60 mm in diameter and 3.0-to 7.5-mm-thick at angles 0°, 45°, and 90° to the bedding. Densities were determined using the submersion method. The sound speeds were determined from the difference in time an ultrasonic pulse took to traverse an aluminum plate and the combination of the same aluminum plate and an oil shale plate. Because of interferences of the ultrasonic pulses at the shale bedding interfaces, only first pulse arrivals were measured. Specifically, an aluminum plate is set between the transmitting and receiving 22-mm-diameter transducers (10 MHz x-cut quartz for longitudinal modes and 5 MHz y-cut quartz for shear modes). The first signal arrival through the plate is set to a fiducial on the screen of a Tektronix 454 oscilloscope. The received pulse is amplified by a Tektronix 461A wideband amplifier. The oil shale specimen plate is placed between the transducers along with the aluminum plate. A suitable oil or resin is used to bond all sample-plate-transducer interfaces. The

first signal arrival is again reset to the fiducial using the time-mark generator-calibrated "delay-time-multiplier" dial of the oscilloscope. The difference in the transit times of the aluminum plate and the plate with shale is determined from the change in the "delay-time-multiplier" dial reading.

Plots of wave velocities for five different propagation modes measured for this assumed transverse isotropic solid are displayed in Fig. 1 as a function of density. Because of the large scatter in the values of any one velocity at a given density, two linear fits having radically different slopes joined at a density of 2.0 Mg/m^3 were chosen to represent each of the velocities as a function of density. The density, 2.0 Mg/m^3 , roughly correlates with the density of 2.14 Mg/m^3 , which is calculated for a close-packed sphere system where the spheres have a density of 2.65 Mg/m^3 (average for the mineral assemblages) and the interstitial material has a density of 1.05 Mg/m^3 (density of kerogen [4]). At densities less than 2.14 Mg/m^3 , according to the model, intimate contact between the mineral grains begins to break down and the velocities reflect those of kerogen containing floating mineral particles.

The linear fits of these 5 velocities, and a description of each are listed below.

$$\begin{aligned} V_1 &= 3.20 + 0.50 (\rho - 1.4) \text{ km/s} & \rho &= 1.4 \text{ to } 2.0 \text{ Mg/m}^3 \\ &= 3.50 + 4.10 (\rho - 2.0) \text{ km/s} & \rho &= 2.0 \text{ to } 2.5 \text{ Mg/m}^3 \end{aligned} \quad (1)$$

V_1 is the longitudinal velocity directed parallel to the shale bedding.

$$\begin{aligned} V_3 &= 2.45 + 0.50 (\rho - 1.4) \text{ km/s} & \rho &= 1.4 \text{ to } 2.0 \text{ Mg/m}^3 \\ &= 2.75 + 4.10 (\rho - 2.0) \text{ km/s} & \rho &= 2.0 \text{ to } 2.5 \text{ Mg/m}^3 \end{aligned} \quad (2)$$

V_3 is the longitudinal velocity directed perpendicular to the shale bedding.

$$\begin{aligned} V_4 &= 1.20 + 0.67 (\rho - 1.4) \text{ km/s} & \rho &= 1.4 \text{ to } 2.0 \text{ Mg/m}^3 \\ &= 1.60 + 2.50 (\rho - 2.0) \text{ km/s} & \rho &= 2.0 \text{ to } 2.5 \text{ Mg/m}^3 \end{aligned} \quad (3)$$

V_4 is both the shear velocity directed perpendicular to the bedding of the shale, and the shear velocity directed parallel to the bedding with particle motion perpendicular to the bedding.

$$\begin{aligned} V_5 &= 2.75 + 0.50 (\rho - 1.4) & \rho &= 1.4 \text{ to } 2.0 \text{ Mg/m}^3 \\ &= 3.05 + 4.10 (\rho - 2.0) & \rho &= 2.0 \text{ to } 2.5 \text{ Mg/m}^3 \end{aligned} \quad (4)$$

V_5 is called a quasi-longitudinal velocity directed at 45° to the bedding.

$$\begin{aligned} V_6 &= 1.70 + 0.50 (\rho - 1.4) & \rho &= 1.4 \text{ to } 2.0 \text{ Mg/m}^3 \\ &= 2.00 + 2.75 (\rho - 2.0) & \rho &= 2.0 \text{ to } 2.5 \text{ Mg/m}^3 \end{aligned} \quad (5)$$

V_6 is the shear velocity directed parallel to the bedding with the particle motion also parallel to the bedding.

The elastic moduli of the shales can be determined as a function of density from the velocity-density relations above and the elastic moduli-density-velocity relations for transverse isotropic or hexagonal symmetry. The bulk moduli range from 5.0 GPa for 1.4 Mg/m^3 , to 7.2 GPa for 2.0 Mg/m^3 , and to 29.6 GPa for 2.5 Mg/m^3 .

In the measurements reported above, porosity was carefully avoided so that a correlation between density and sound speed could be established. The effect porosity and water saturation has on sound speeds and elastic moduli was measured on a highly porous (12%), low kerogen-content oil shale from the Anvil Points Mine. The sound speeds of 30 samples cut at 0° , 45° , and 90° to the bedding were determined both dry and saturated with water.

These measurements showed that the 12% porosity appears to have lowered velocities between 14% and 23% (V_1 -21%, V_3 -17%, V_4 -14%, V_5 -17%, V_6 -23%). Filling the pores with water further lowered the longitudinal velocities by 10% and the shear velocities by 20%. The porosity apparently lowered all elastic moduli by 35% to 45%. The "diagonal" moduli further

decreased when the shale was saturated, but the "off-diagonal" moduli increased as did the bulk modulus.

The velocities and moduli of the end members of the oil shales, the kerogen and the mineral assemblages, can be projected from the velocity fits. If the density of kerogen is assumed to be 1.05 Mg/m^3 , then using the velocity fits for the lower density shales, the bulk modulus of kerogen is calculated to be 3.64 GPa ($V_\phi = 1.86 \text{ km/s}$). If the density of the mineral assemblage is assumed to be 2.65 Mg/m^3 , then using the velocity fits for the higher density shales, the bulk modulus of the assemblage is calculated to be 40.3 GPa ($V_\phi = 3.90 \text{ km/s}$).

DYNAMIC TENSILE STRENGTHS

In a shock wave's divergent propagation from both spherical and cylindrical detonations, the initial positive compression rapidly converts into tension, particularly the tangential component. This dynamic tensile stress is a major contributor to the fracture of the surrounding rock. Another form of fracture, though minor, caused by dynamic tensile stress is spalling. Spalling occurs behind a free surface at which a finite shock wave releases; the resulting rarefaction wave from the free surface and rarefaction wave following the shock collide and form a spreading tension wave. Thus, the dynamic tensile strength of rock is an important property to be determined when attempting to predict the fracture pattern of a rock in response to detonation. Here two techniques are described for determining the dynamic tensile strength of oil shales; the results of studies using these techniques are presented.

The first technique involves the determination of the velocity profile of the free surface of a plate of oil shale which has been impacted. This is done by monitoring the change in capacitance between the free surface of

the oil shale on which has been deposited a thin (1000 \AA) metallic coat and a polarized parallel plate. The associated electronic circuit is designed so that the signal voltage is proportional to the time rate of change of the capacitance.

In this experiment the stress wave resulting from plate impact pass through the shale until the front of the stress wave reaches the free surface. There the free surface moves out from its static position at a velocity approximately equal to the impact velocity. An example of a history of free surface motion interpreted from a capacitor record is shown in Fig. 2. The stress is relieved at the free surface and a release wave propagates back toward the surface of impact. When the rarefaction wave following the stress wave and the release wave from the free surface collide, a tension stress is created which begins to propagate toward both the surfaces. If the tension at the point of collision creates a spall immediately, the tension wave goes no further, and the free surface continues to move out at a constant velocity equal to the impact velocity. However, if the tension does not cause spall immediately then at least part of the tension stress wave reaches the free surface resulting in a slow-down of the surface velocity. If no spall occurs while the entire sample is under tension, the free surface will return to zero velocity. The amount of velocity reduction is proportional to the magnitude of the tensile strength. If the experiment propagated a 0.7-GPa stress pulse through the shale, and the free surface velocity was reduced by 50% before the spall stress reached the rear surface, then the tension which caused the spall was approximately -350 MPa.

For the series of experiments conducted on three orientations of shale at three impact velocities and various densities, the spall strength can be

estimated to be the order of -100 to -200 MPa. No more detail than this could be obtained from the limited number of experiments conducted.

The second technique involves impacting shales of known shock impedance and orientation to bedding with a thin driver of known shock impedance generating a well defined shock in the shale. The impedance of the impactor plate is chosen so that the interface between the impactor and the sample separate after passage of the rarefaction wave from the rear free surface of the impactor. Again, as in the previous technique, the rarefaction from the impact surface of the shales and their other surface, which is free, collide in the middle region of the shale samples creating a tension wave. The target plate in which the shale samples are mounted is recovered and the shales are removed and examined for spall. The experimental configuration is shown and described in Fig. 3.

The impactor plate used is Plexiglas, $\rho_o = 1.186$, its thickness chosen to cause collision of the rarefactions midway through the oil shale. Since the shock velocity in shales are within a few percent of their elastic longitudinal velocities at these stress levels, it was assumed the stress induced in the oil shale samples is approximately

$$P(\text{GPa}) = \rho \text{ (Mg/m}^3\text{)} \times C_L \text{ (km/s)} \times u_p \text{ (km/s)} \quad (6)$$

where ρ is the density of the shale, C_L is the measured elastic longitudinal velocity, and u_p is the particle or interface velocity between the Plexiglas and shale. Since the stress levels induced were approximately 100 MPa (0.1 GPa, 1 kilobar), the stress induced in the Plexiglas impact plate is approximately

$$P(\text{GPa}) = \rho \text{ (Mg/m}^3\text{)} \times C_B \text{ (km/s)} \times (u_D - u_p) \text{ (km/s)} \quad (7)$$

where ρ is the density of the plexiglas, C_B is the bulk elastic velocity

as determined from the Plexiglas Hugoniot ($C_B = 2.598$ km/s), u_D is the particle or interface velocity before impact and u_p is the particle or interface velocity. At impact, both the stress and the interface velocity in the oil shale and the Plexiglas at the interface are the same. If the shock wave in the oil shale is not overtaken by the release wave, and the thickness of the impact plate is such as to prevent this, the magnitude of the maximum tension induced in the oil shale should nearly equal the maximum stress induced in the shale.

$$\text{Tension} = -u_D \frac{(\rho_{o.s.} \times C_{L o.s.}) \times (\rho_{\text{plexy.}} \times C_B \text{ plexy.})}{(\rho_{o.s.} \times C_{L o.s.}) + (\rho_{\text{plexy.}} \times C_B \text{ plexy.})} \quad (8)$$

where the o.s. subscript denotes oil shale and plexy. denotes Plexiglas. Both the density and elastic longitudinal velocity of each shale sample are determined before each impact experiment, and the impact plate velocity is determined during the experiment (Fig. 3), thus the tension induced in each sample can be readily calculated.

The diagnosis of an impact experiment is straightforward. The target plate is recovered in a large rag-filled tank, its back is removed and the oil shale samples are pressed out. Each shale is examined for spalling. If the sample spalled into two or more pieces, it is denoted by a dark circle in Fig. 4. If a crack formed across the mid-plane of the sample, but the two halves can not be readily separated from each other, the experimental point is denoted by a half filled circle. If the sample remains whole, it is denoted by an open circle. Figure 4 summarizes the results. Here the tension induced in the samples are plotted as a function of the shale's density. The three plots are for each of three orientations studied. (See caption for explanation of orientation).

Six different sets of shale were studied for their dynamic tensile strengths; one set had a density of approximately 1.85 Mg/m^3 , one set had densities slightly greater than 2.0 Mg/m^3 , two sets had densities in the vicinity of 2.2 Mg/m^3 , and two sets had densities near 2.35 Mg/m^3 . Only general conclusions can be derived from Fig. 4. The shales with orientation $\theta = 0^\circ$ are only slightly stronger than those with orientation $\theta = 90^\circ$. As the two sets of shales having densities near 2.2 Mg/m^3 clearly show, tensile strengths can vary widely for a given density. It is not possible to resolve a dependence of the tensile strength on density. The results do show that for these six sets of shales, the tensile strengths fall somewhere between -130 MPa and -30 MPa.

Felix (5) conducted dynamic tensile strength tests on similar shales and found them to be about -10 MPa for $\theta = 90^\circ$ and -35 MPa for $\theta = 0^\circ$ at a density of about 2.2 Mg/m^3 . For a similar density the present results give -20 and also -100 MPa for the two sets at 90° and -50 and also -110 MPa for the two sets at 0° . The tensile strengths found here are considerably larger than those found by Felix. The major differences in the two investigations is the stress rates involved and the duration of the tension. The stress rates for the two techniques described here are about $-1 \text{ GPa}/\mu\text{s}$. The tensile stress rates in the experiments by Felix are $-0.6 \times 10^{-3} \text{ GPa}/\mu\text{s}$. In addition, his material remains under tension for as long as 50 to 60 μs , while the shales for the present experiments are under tension for only about 2 μs . Obviously, the magnitude of these differences could account for the observed differences in tensile strengths.

RESPONSE TO PLANE STRESS IMPULSES

Properties of oil shales to dynamic stress can best be determined from the analysis of the degradation of finite stress impulses as they pass through the shales. Various techniques and analyses are currently used by various laboratories, mainly originating at the Stanford Research Institute

and the Sandia Laboratory at Albuquerque.

The technique used here is to measure the stress history of an impulse at several depths in a shale sample. The sample assembly consists of a stack of shale plates all 40-mm in diameter. The first plate is 2-mm-thick, the second and third plates are 4.5-mm-thick; and the fourth is 5-mm-thick. The impactor plate is usually 3-mm-thick. The density, elastic properties, and orientation of all plates are matched. Between the shale plates of the sample assembly are 50-ohm grids of 0.01-mm-thick manganin foil that cover an area of 40 mm^2 in the center region of the plates. The resistance of the grids are well defined as a function of stress under impact conditions. The resistance is deduced from the voltage generated at the null point of a pulsed Wheatstone bridge caused by the change in resistance of the manganin grid. The sample-manganin gage stack is placed in a target plate and surrounded by velocity pins. The entire assembly looks much like that in Fig. 3 except that the 6 small samples are replaced by the stack, and the Plexiglas plate mounted on the hollowed Al projectile is replaced with a shale impactor plate.

In the upper left diagrams of Figs. 5, 6 and 7 are stress histories recorded in three experiments on oil shales. The differences between the experiments are the orientation of the bedding to the direction of planar shock propagation, and the shale densities. The response of the shales to the shock loading and unloading was calculated using a computer code, GUINSY2, written by Lynn Seaman of Stanford Research Institute. The theory on which the code is based and an explanation of how the code is used was earlier described by Seaman (6). The

analysis requires the stress histories, correlation of regions on the stress profiles, the initial density of the shales, and the initial gage locations. From the analysis the specific volume, the particle velocity, and internal energy of the shales are correlated with the stress as a function of time at each gage location. In the remaining diagrams of Figs. 5, 6, and 7 are plotted particle velocity as a function of the loading and unloading stress, strain as a function of the loading and unloading stress, and the loading and unloading wave velocity as a function of particle velocity.

These three sets of diagrams represent the responses of only three combinations of many; other experiments and analyses have been completed at the same three orientations on other densities of shales at other stress levels. These are available from the author. Here the general character of the response of the shale to impact is described.

At stress less than 1 GPa, as illustrated here, no distinct elastic wave could be detected moving out from the shock front; this normally occurs in the shock-loaded deformation of solids that undergo elastic-plastic yielding. The shock profiles do exhibit some dispersion with the stress rise times increasing with distance. This indicates that the shale yields gradually under shock compression and also manifests itself in the curvature of the stress-particle velocity and stress-strain plots on loading. It is also indicated by the decrease in the loading wave velocity with increasing particle velocity or stress. Several investigators have proposed yielding models for this phenomenon (3), (7), (8), but models for the response of oil shale to shock compression are beyond the scope of this study. The stress rise time at stress levels of the order of 3 GPa exhibit no dispersion

showing that the shock wave had overrun the elastic component.

The velocities of the shock waves at stresses less than 1 GPa have the same value as - or are several percent smaller than the velocity of the longitudinal wave, again indicating a strong elastic component. This also means that at low stress levels the shock wave velocity depends strongly on shale density and orientation. The rarefaction velocities or unloading wave velocities are 20% to 30% faster than the shock velocities except for the 30° orientation where the initial shock velocity is only several percent slower than the rarefaction velocity, but the velocity of the shock front decreases rapidly with increasing stress. The unloading wave velocities at higher stresses, 2 GPa to 3 GPa, are 50% to 80% faster than the loading wave velocity.

The stress-strain plots in Figs. 5, 6 and 7 are stress-compression ($1 - V/V_0$) plots, but the assumption made is that all the compression is uniaxial with no lateral particle motion involved. The greatest stress-strain hysteresis is exhibited by planar impact perpendicular to the bedding, and the extent of the hysteresis decreases with the angle to the bedding. It is not known if the extent of hysteresis can be correlated with permanent deformation since complete unloading is not measured with the techniques used here. The data is not sufficient to correlate the width of the stress-strain hysteresis with oil shale density.

ACKNOWLEDGMENT

The author would like to thank Lynn Seaman and Bonnie Lew of Stanford Research Institute for contributing their code, GUINSY2, and for taking time to give instructions concerning its operation. The author wishes to recognize the efforts of Al Lopez, Chuck Caldwell

and Bill Smith of Group M-6 at Los Alamos for sample preparation, sample assembly, and operation of the air gun. Acknowledgement is given to the Energy and Research Development Administration for their support.

REFERENCES

1. M. E. Chenevert and C. Gatlin, Mechanical anisotropies of laminated sedimentary rocks, Soc. Petrol. Engrs. Jour., March, (1964).
2. R. N. Schock, B. P. Bonner and H. Louis, Collection of Ultrasonic Velocity Data as a Function of Pressure for Polycrystalline Solids, UCRL-51508, Lawrence Livermore Laboratory, Livermore, California, (1974).
3. J. N. Johnson, Dynamic Anisotropic Constitutive Relations for Oil Shale, TR 75-25, Terra Tek, Salt Lake City, Utah, (1975).
4. J. W. Smith, Theoretical Relationship Between Density and Oil Yield for Oil Shales, Report of Investigation 7248, Bureau of Mines, U. S. Dept. Interior, (1969).
5. M. P. Felix, Determination of Stress Levels for Dynamic Fracture of Oil Shale, a report from the School of Aeronautics and Astronautics, Purdue University, West Lafayette, Indiana 47907,
6. L. Seaman, Lagrangian analysis for multiple stress or velocity gages in attenuating waves, J. Appl. Phys., 45, 4303-4314, (1974).
7. D. E. Grady, R. E. Hollenbach, K. W. Schuler, and J. F. Callender, Strain rate dependence in dolomite inferred from impact and static compression studies, J. Geophys. Res. 82, 1325-1331, (1977).
8. J. C. Nunziato, E. K. Walsh, K. W. Schuler, and L. M. Barker, Wave propagation in nonlinear viscoelastic solids, in Handbuch der Physik, Vol. 6a, Part 4, ed. by C. Truesdell, (Springer, New York) (1975).

TABLE 1. Composition of Oil Shales from the
Anvil Points Mine, Rifle, Colorado

Whole Shale	Dolomite	Quartz	Analcime	Calcite	Albite	Kerogen	
Density (Mg/m ³)	2.85	2.65	2.25	2.65	2.62	1.05	
	Vol.% ^a	Vol.% ^a	Vol.% ^a	Vol.% ^a	Vol.% ^a	Vol.% ^b	Wt.% ^b
1.530	35	25	25	~ 0	15	69	47
1.570	35	25	25	~ 0	15	67	45
1.760	45	28	17	~ 0	10	56	34
1.760	43	20	30	~ 0	7	55	33
1.878	45	23	22	~ 0	10	49	28
1.893	45	23	22	~ 0	10	48	27
1.946	35	25	20	15	5	44	24
2.028	43	20	~ 0	10	27	42	22
2.040	43	20	~ 0	10	27	41	22
2.055	35	25	20	15	5	37	19
2.177	35	25	20	10	10	29	14
2.307	34	34	8	8	16	23	11
2.520	30	22	13	13	22	8	3

- a. An estimate of the volume percent from among the crystalline constituents, based on x-ray powder diffraction patterns.
- b. The volume and weight percents of kerogen for the whole shale calculated from the sample density and the calculated density of the mineral constituents, always between 2.6 and 2.7 Mg/m³ for these shales.

Fig. 1. Elastic wave velocities in transverse isotropic oil shales having densities ranging from 1.4 Mg/M^3 to 2.4 Mg/m^3 .

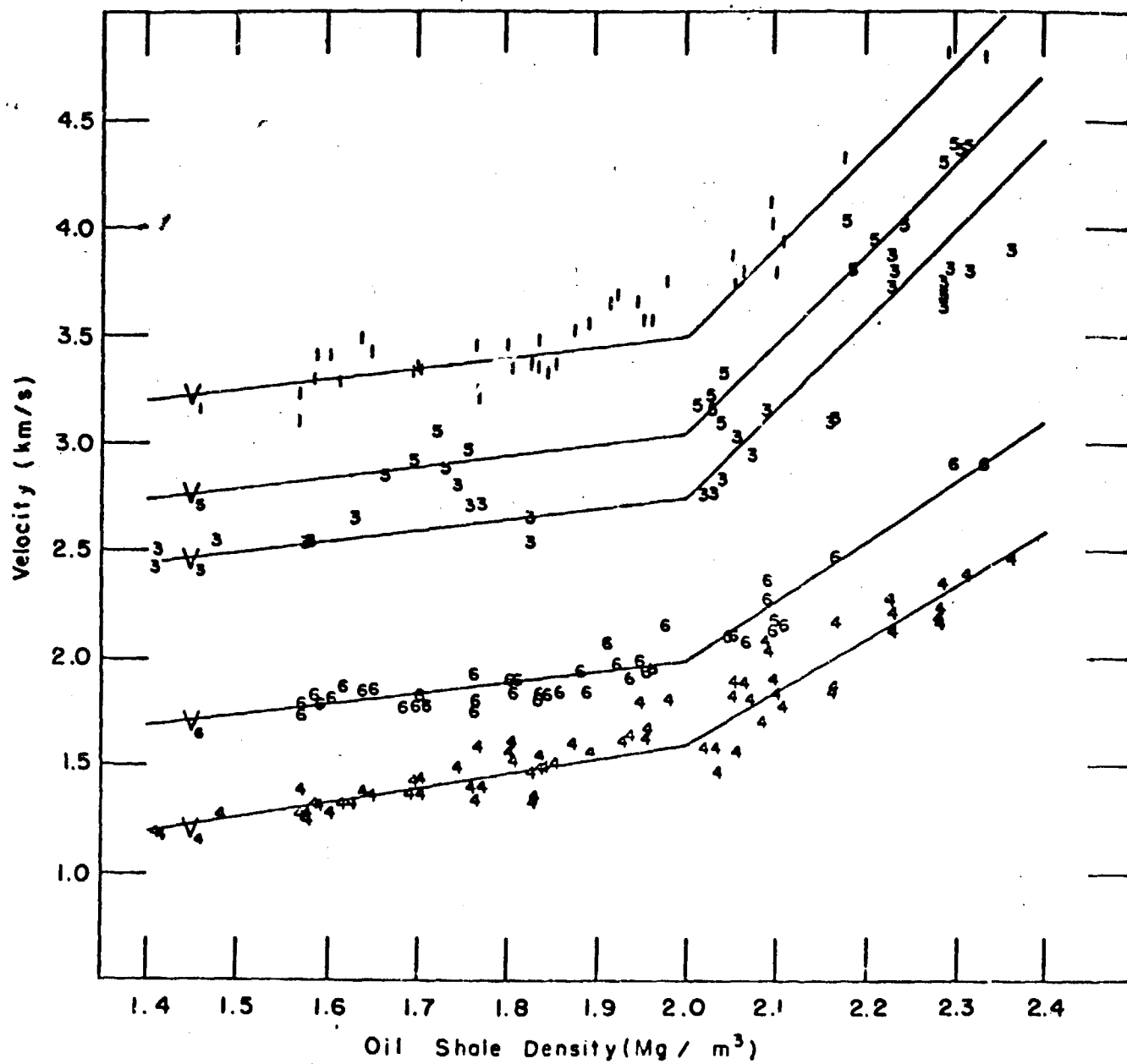


Fig. 2. The free surface velocity of an oil shale plate that has been impacted with a thin plate of similar material. The history was deduced from data recorded by the capacitor technique.

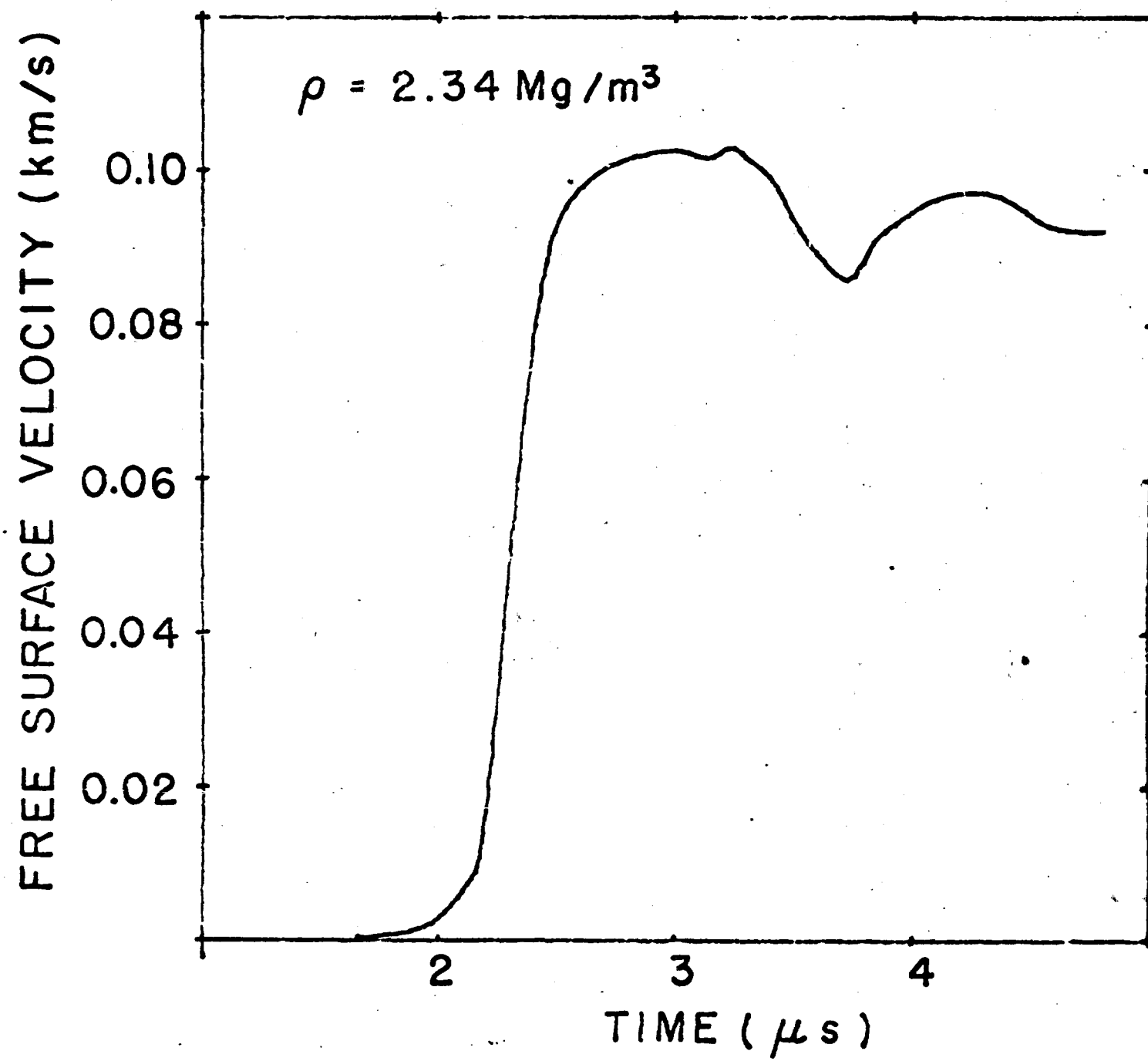


Fig. 3. A front view of a target plate (a) and a cross-sectional view of an impact experiment (b). The view, (a), shows the arrangement of the shale samples in the target plate, machined from Al. Six samples, D, of different densities and orientations are mounted in the target plate, B. Each sample is backed with low density (0.015 Mg/m^3) plastic foam, H, to facilitate mounting the specimens' impact surfaces flush with the target plate's surface. The specimens are held in the plate with a thin layer of epoxy. Shorting pins, C, of various lengths are used to determine the velocity of the impact plate, G. The front surface of the impact plate is covered with a 0.01 mm thick Al foil shorted to the projectile, E. A pulse is generated on a repetitive time-marked oscilloscope sweep as each charged pin is shorted. The muzzle of the 3 m long, high pressure gas gun used to drive the projectile is labeled A, the target plate mounting screws are labeled I, and the unsupported area behind the impact plate is labeled F.

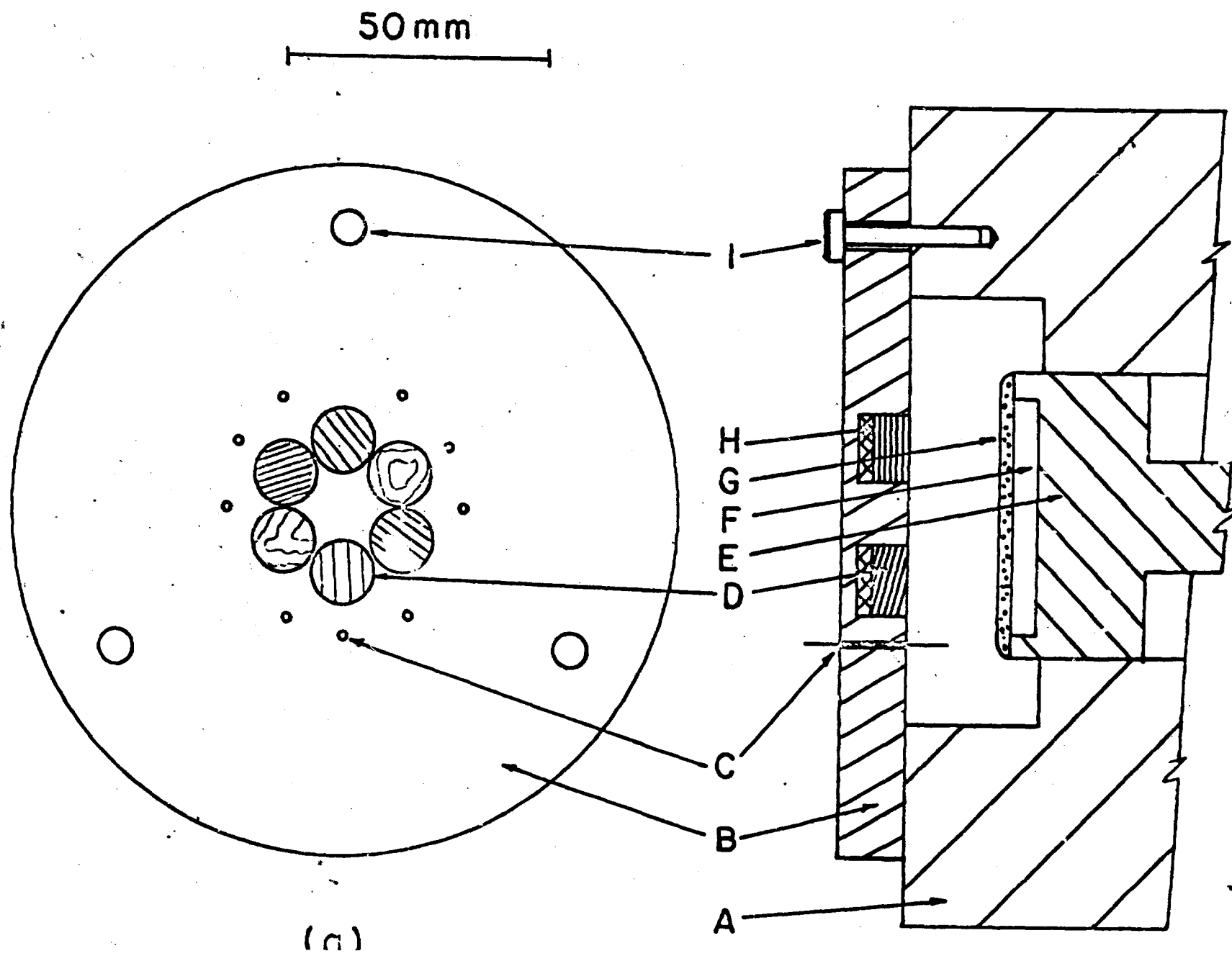


Fig. 4. The tension to which the oil shale samples of various orientations, $\theta = 0^\circ$, 45° and 90° , and densities were subjected. For $\theta = 0^\circ$, the bedding of the shale was perpendicular to the plane of impact or parallel to the direction of impact. For $\theta = 45^\circ$, the bedding was at 45° to both the plane of impact and direction of impact. And for $\theta = 90^\circ$, the bedding was parallel to the plane of impact and perpendicular to the direction of impact. The open circles denote no fracture, the half circles indicate that the samples cracked but didn't completely fracture, and filled circles denote that fracture occurred.

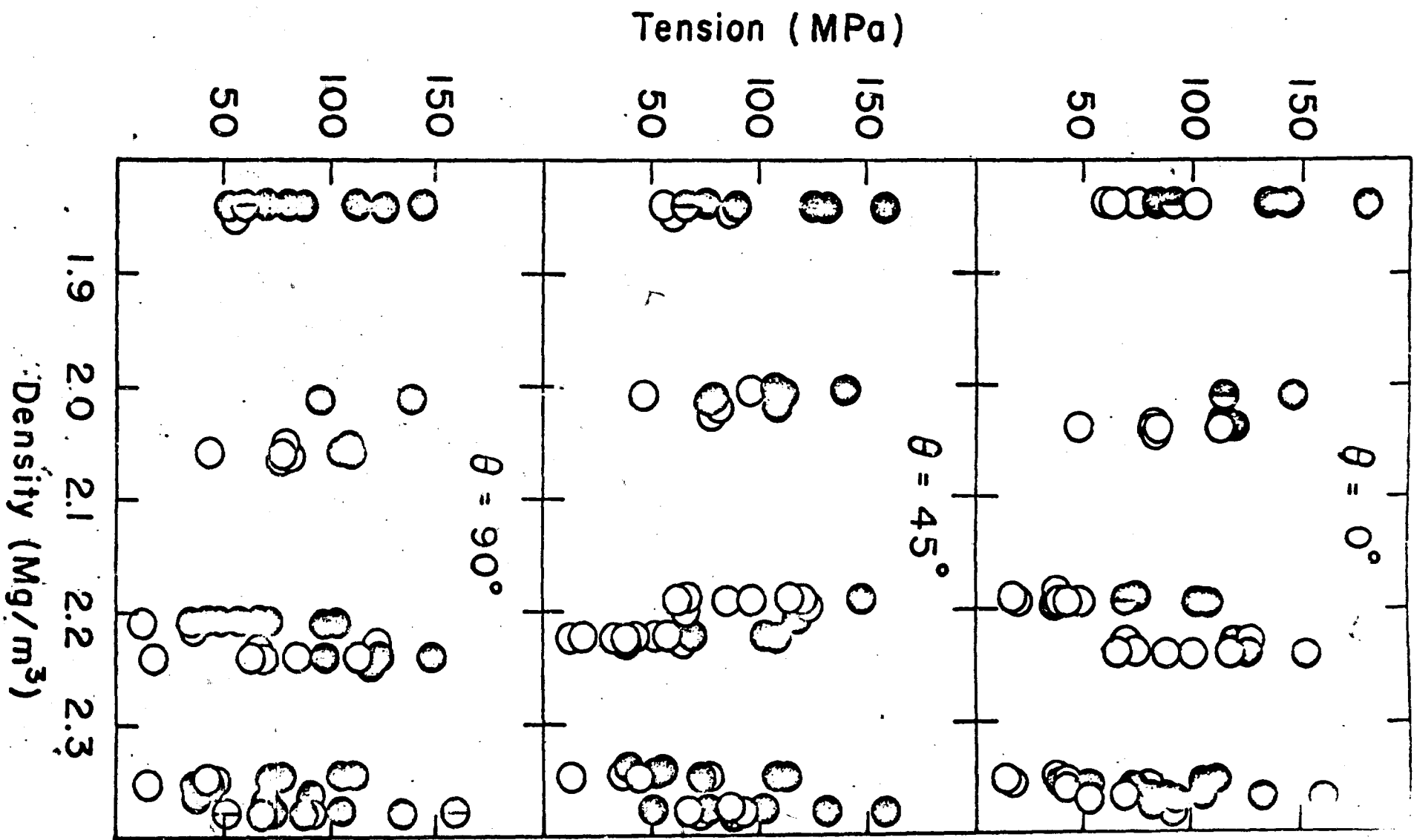


Fig. 5. Response of oil shale ($\rho = 1.89 \text{ Mg/m}^3$, $\theta = 0^\circ$)
to planar shock loading and unloading.

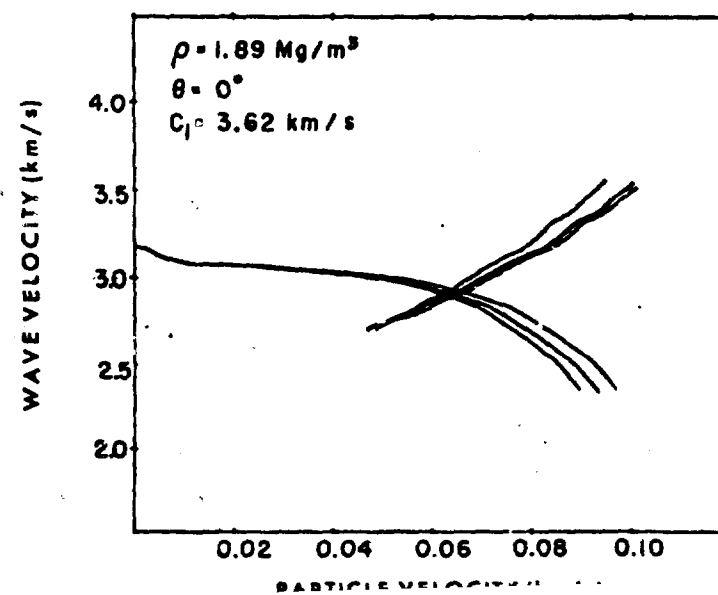
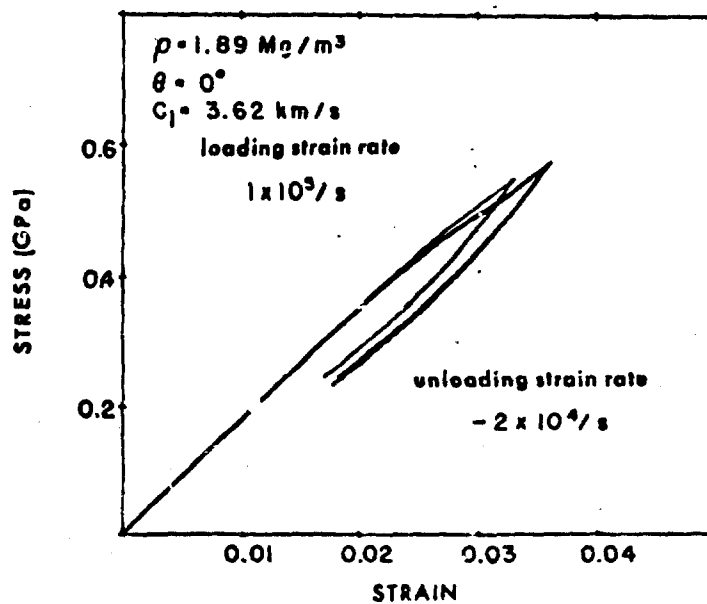
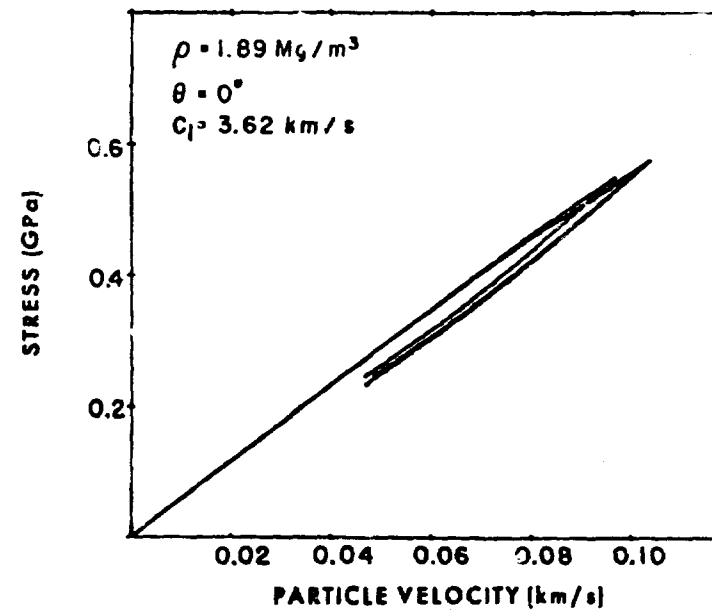
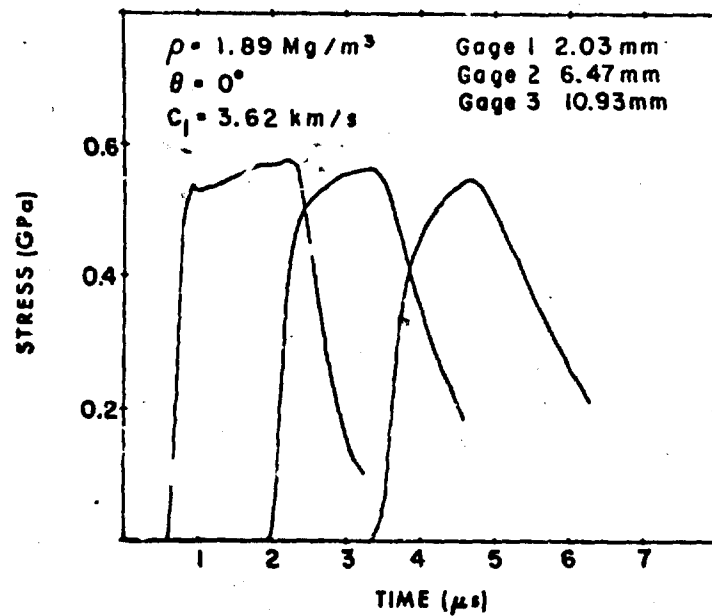


Fig. 6. Response of oil shale ($\rho = 2.19 \text{ Mg/M}^3$, $\theta = 30^\circ$)
to planar shock loading and unloading.

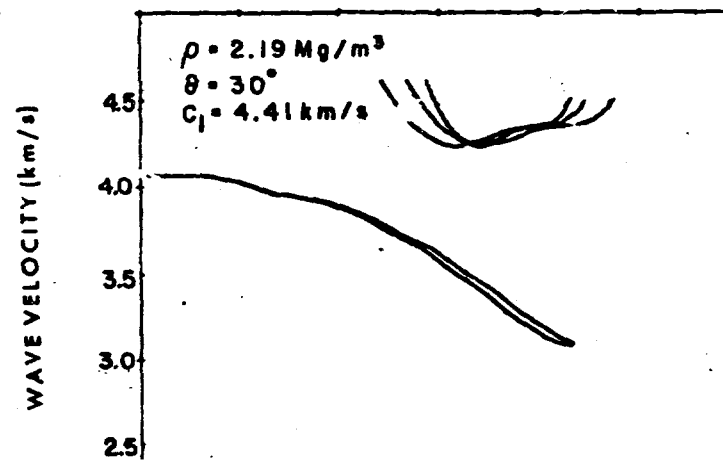
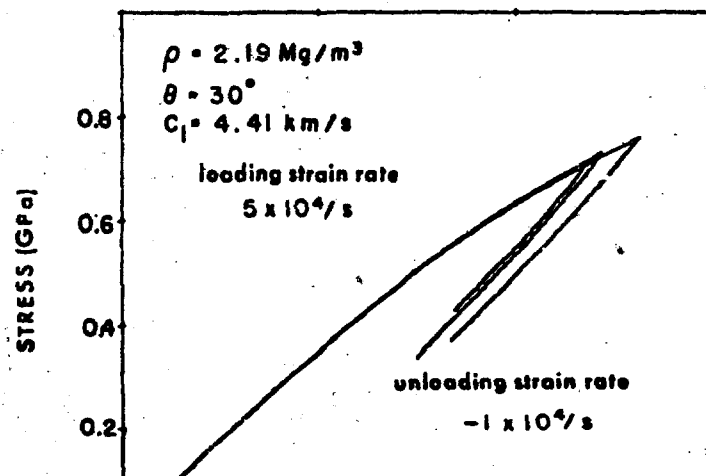
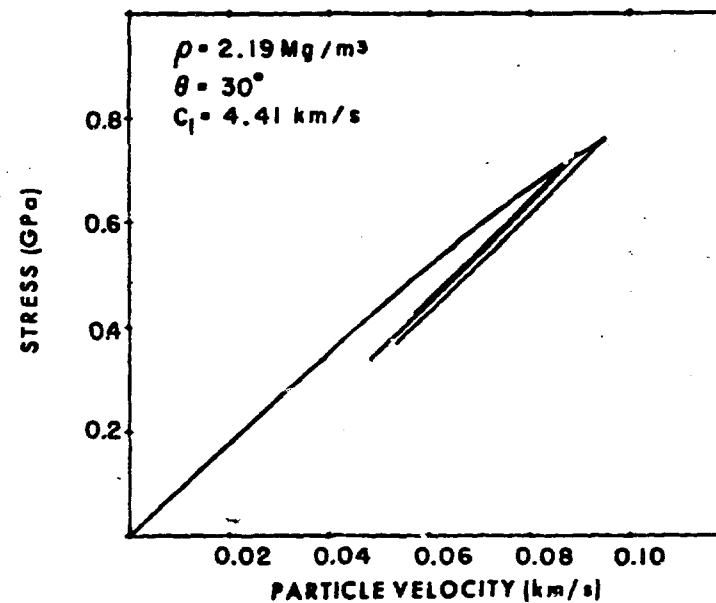
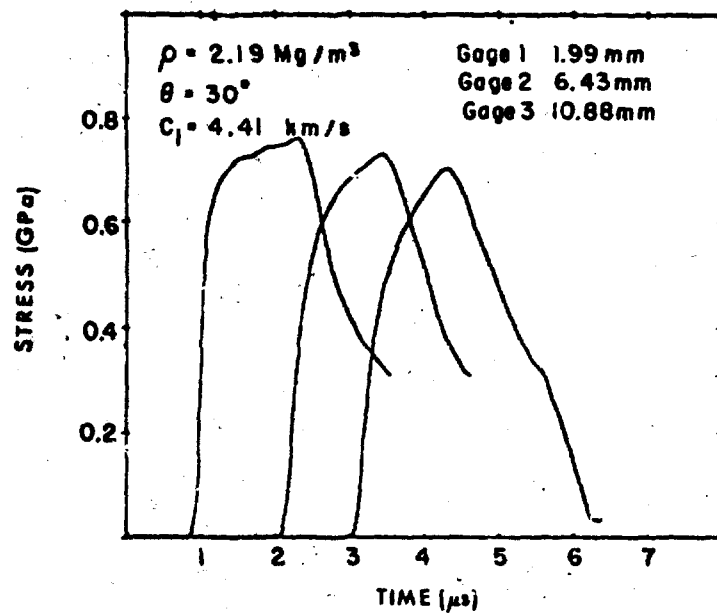


Fig. 7. Response of oil shale ($\rho = 2.08 \text{ Mg/m}^3$, $\theta = 90^\circ$)
to planar shock loading and unloading.

